

Magdalena Ridge Interferometer: assembly, integration and testing of the unit telescopes

Olivier Pirnay^a, Maxime Pierard^a, Vincent Moreau^a, Peter Verheyden^a, Chris Mayer^b

^aAdvanced Mechanical and Optical Systems (AMOS s.a.),
LIEGE science park, B-4031 Angleur, BELGIUM;

^bObservatory Sciences Ltd, William James House, Cowley Road, Cambridge, CB4 0WX, UK.

ABSTRACT

AMOS is in charge of the development of the unit telescopes for the MRO interferometer. This paper depicts the progress of the project and presents the results of the factory acceptance tests that were performed at AMOS facilities. Those tests are the earliest verifications of the telescope performance. AMOS has now extensive experience in testing small and large instruments, including optical testing, alignment, mechanical static, dynamic measurements, system identification, etc. It is this combination of various techniques of measurement that produce accurate and reliable results.

Keywords: telescope, interferometry, optical array, testing, identification, optical path length stability, elevation over elevation

1. INTRODUCTION

The Magdalena Ridge Observatory Interferometer (MROI) is a high-sensitivity imaging optical/IR interferometer in construction on the Magdalena Ridge. It is situated at the altitude at 3230 m, 45 km West of Socorro, NM.

Up to 10 unit telescopes will be operated simultaneously to produce model-independent images. These telescopes can be relocated on 28 different piers spread on a "Y" shape array. With baselines from 7.5 m to 340 m, the instrument will generate sub-milliarcsecond angular resolution sharp images in the range of 0.6 to 2.4 μm wavelength.

The instrument optical throughput is optimized in order to image faint objects: one key piece is the 1.4 m unit telescope in which the stellar light is collected with only three mirrors possible due to the afocal elevation over elevation configuration.

The major science goals are the study of the earliest phases of star and planet formation, the complex astrophysical processes in single and multiple star systems, and the environments of black holes in the hearts of other galaxies.

The design of all major systems for the interferometer has been completed. AMOS has concluded the manufacturing of the first unit telescope and it is now in its final stage of testing in Belgium. Orders have also been placed for the long lead items of the second and third telescopes. Construction of the Beam Combining Facility (BCF) which facility includes the interferometric laboratory, the delay line area, control room and administrative space, has been completed. The design of the enclosure is finished and the RFQ for fabrication has been issued.

*olivier.pirnay@amos.be; phone 32 4 361 40 40; www.amos.be



Fig. 1. Artistic view of the MRO Interferometer in closed packed configuration. The buildings construction was completed in 2007. (Courtesy of MRO)

2. TELESCOPE DESIGN OVERVIEW

2.1 Requirement specifications

The telescope is a Mersenne beam compressor supported by an elevation-over-elevation mount. The system consists of a 1425 mm diameter $f/2.25$ concave parabolic primary combined with a 115 mm diameter convex parabolic secondary. The M1-M2 spacing is 2936.25 mm. The 95 mm diameter collimated beam is sent out of the telescope through the outer elevation axis due to a flat mirror (M3) rotating around the inner elevation axis. The tracking speed of the M3 is half of the speed of the inner elevation axis. The angular range (field of regard) is $-50/+40$ degrees and ± 60 degrees from zenith for the inner elevation axis and the outer elevation axis respectively.

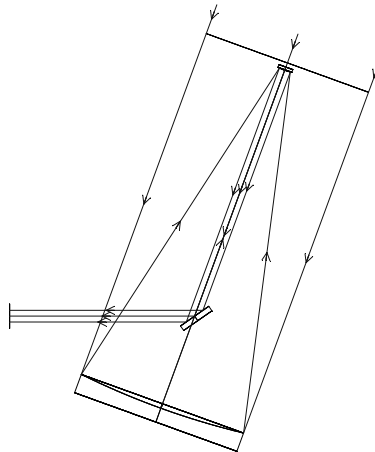


Fig. 2. Optical configuration of the MROI unit telescope.

The ambitious objectives of the MRO Interferometer led the system architects to specify stringent requirements for the unit telescope. The performance summarized here below will be maintained in severe environmental conditions.

- Overall image quality: 63 nm RMS
- Optical obscuration less than 5%
- Pupil stability: 0.5 mm over the entire field of regard
- Pointing error less than 20 arcsec over the full night
- Open loop tracking better than 1 arcsec
- Closed loop tracking: 0.02 arcsec and 0.03 arcsec RMS respectively for the mount and the wind shake residual error. A 200 Hz bandwidth fast steering actuator is implemented at the level of the secondary mirror for tip-tilt correction.
- Optical Path Length (OPL) Stability: 23 nm RMS for a 12 ms exposure time frame

2.2 Mount design

The two axes of the elevation-over-elevation mount are connected to each other by means of a gimbal structure. The fork is the fixed part of the telescope. It supports the outer elevation axis of the gimbal and provides a stiff and stable interface with the pier. The fork also provides the interface for the Nasmyth table where the closed loop sensors are installed by the final user. The gimbal is a closed frame box structure. It locates the two main axes concurring and perpendicular to each other. The gimbal supports the telescope tube through the inner elevation axis. The tube supports and maintains stability of the M1, M2 and M3 units in the entire operational range.

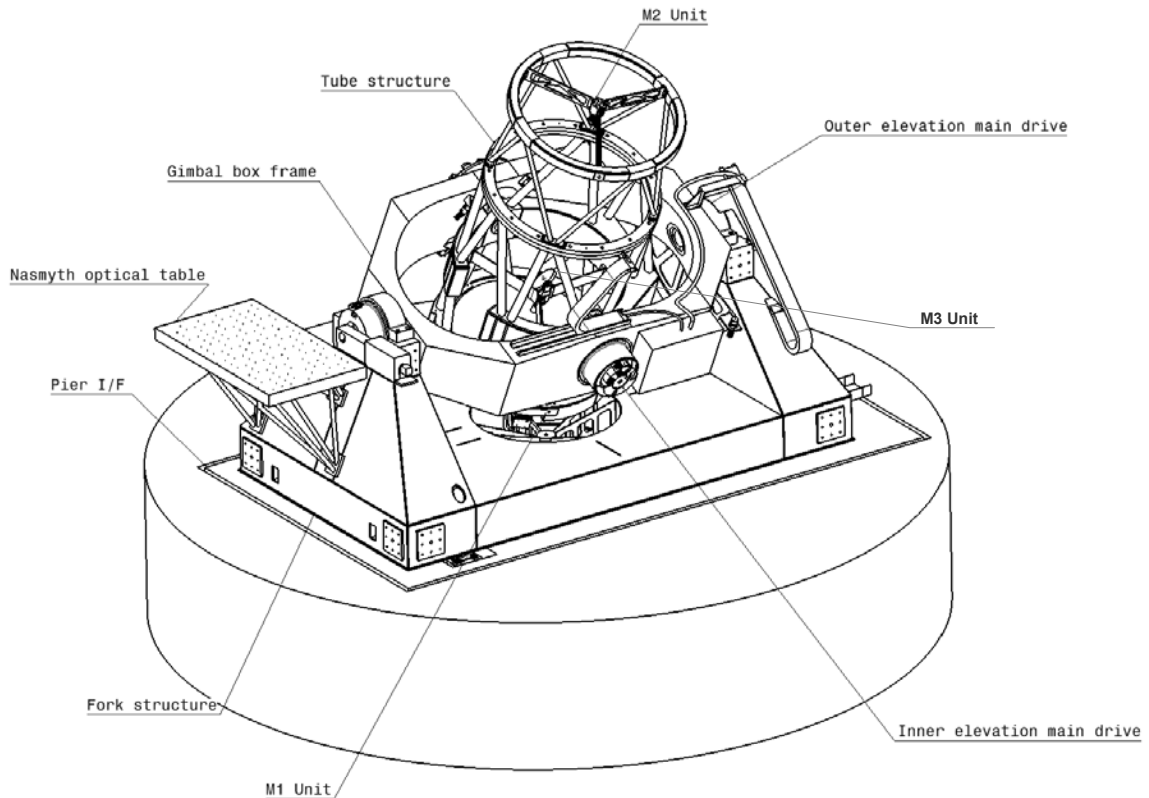


Fig. 3. MROI unit telescope, overall view.

Total weight: 15 500 kg – Overall dimensions (L x W x H): 6160 x 2920 x 4350 mm.

The throughput of the telescope is greatly enhanced by the fact that only three reflections occur from the primary mirror to the output collimated beam. As a drawback, the elevation-over-elevation mount necessitates a large free opening in the tube to avoid any obscuring of the output beam.

The interface with the pier is designed as a kinematic support in order to avoid inducing stress and deformation to the telescope structure in case of misalignment or instability of the pier interface. It also allows accurate re-positioning of the telescope after relocation on another pier of the array.

As the inertia and wind exposure are the same order of magnitude for both axes, the components of each axis are identical except for the bearings. The servo controller is a UMAC Delta Tau dedicated to the main axes. Two liquid cooled DC brushless motors are implemented on each axis (one on each shaft). The UMAC is connected to the SERVOSTAR[®] motor drives through an analog current input. The absolute position feedback is given by a resolver and the high accuracy position feedback is provided by a circumferential-scale drum encoder with four scanning heads. The signal interpolation is performed by a dedicated card in the UMAC.

The unit telescope control system (UTCS) is developed with the LabView[®] programming language^[3]. The kernel of the system makes use of the TCSpk from TPOINT[™]. Pointing directions and trajectories are downloaded to the axis servo-controllers as position set points related to absolute time. A graphical user interface is provided for engineering operation e.g. in stand-alone mode. In the normal operation mode, the UTCS is under the control of the interferometer control system (ICS) via a dedicated socket server.

2.3 Key features

The design of the telescope mount was driven by four constraints: the tracking performance, the optical pathlength stability, the pupil stability and the image quality. The first two are affected by the dynamic behaviour of the system while the last two are influenced by static or quasi-static structural deformation only.

The tight specifications necessitated extensive optimizations and an accurate control of the error budgets. The dynamic performance could be met only by maximizing the natural frequencies of the structure and a proper optimization of the control system. Trade-off analyses and numerous iterative FEM optimizations were necessary in order to meet the image quality and pupil stability requirements. As a result, a compensation strategy based on the change in position of M2 as a function of the temperature and the pointing direction is implemented. This enables the telescope to maintain the image quality, the pupil stability and the pointing accuracy under control in the entire field of regard and temperature operational range.

The compensation law is at first elaborated by analysis and later adjusted with real measurements of the image quality by means of a retractable wavefront sensor that will be used as a calibrator.

A comprehensive presentation of the unit telescope design and the engineering approach are discussed in [2].

3. ASSEMBLY AND INTEGRATION

The functionality and the performances of the telescope are related to the proper form fit and function of the individual components. Depending on the complexity and the criticality of the system, the tests and inspections are conducted either by the supplier or by AMOS. The mechanical parts are inspected before assembly in the telescope. The sub-systems such as the mechanisms are also tested before integration.

At each step of the assembly, the features of the assembly that have an impact on the final performance or functionality are measured or tested. Their compliance with the error budget, as shown in Table 1, is verified. The major items are the bearings and shafts alignment, the run-out of the inner and outer elevation axes, the centering of the inner axis with respect to the outer axis, the coincidence of the M3 axis with respect to the inner axis, the centering of the tube with respect to the telescope pivot point and the pier interface localization.

During the integration phase, numerous dimensional controls were performed prior to the assembly in order to insure that the parts were manufactured with the required dimensional tolerances.

Following the completion of the integration phase, the telescope is now in the process of undergoing the factory acceptance tests. Amongst others, the smooth, accurate and dynamically stable operation of the main axes necessitates a good balancing of the structure and a fine tuning of the control loops. The alignments have been performed and all the functionalities successfully tested.

Table 1. Alignment tolerances

Error source	Ref frame	DOF	Tolerances	Completion method	Verification method
M1 – M2	Optical	Dx	42 μm	Mechanical pre-alignment of M1 and M2	WFS measurement
		Dy	42 μm		
		Dz	2.2 μm		
		Tx	42 arcsec		
		Ty	42 arcsec		
M3 vertex – M3 axis	M3	Dz	10 μm	Alignment	Metrology
		Tx	5 arcsec		
M3 axis – Inner axis	Optical	Dx	50 μm	Alignment	Metrology theodolite and laser tracker
		Dz	50 μm		
		Tx	10 arcsec		
		Tz	10 arcsec		
Inner axis – Outer axis	Gimbal	Dy	50 μm	Manufacturing	Metrology theodolite and laser tracker
		Dz	50 μm		
		Tz	10 arcsec		
Optical axis – pivot point	Gimbal	Dx	100 μm	M1 alignment	WFS measurement with M2 vertex align on pivot point
		Dy	100 μm		
		Tx	10 arcsec		
M3 axis runout		R_{M3}	5 μm	Manufacturing specifications and mounting	Metrology theodolite and laser tracker
Inner axis runout		R_{in}	20 μm		
Outer axis runout		R_{out}	20 μm		
Pier Stability	Telescope	Tx	7.9 arcsec	Specification toward Pier design	Survey equipment
		Ty	5.1 arcsec		
		Tz	15.7 arcsec		

3.1 Main axis alignment

The performance in terms of pupil stability depends on the relative position of the main axes. This is essentially given by the accuracy of manufacturing of the gimbal. This was measured before and checked after integration of the gimbal on the fork.

An accurate centering of the gimbal and the tube with respect to the central pivot point of the fork is performed by adjustment of large shims between the bearings and the structures.

The position of each axis is determined by measuring the position of the corner cube installed on the gimbal or the tube while the part is rotating around its axis. This technique is usual to align the axes and measure the bearing run-out.



Figure 4. Main axes measurement by means of the laser tracker (laser beam sketched over the picture)

3.2 M3 mechanism alignment

The co-alignment of M3 mechanism axis with respect to the inner elevation axis is the major contributor to the pupil stability; this is due to the fact that it acts as a lever arm on the pupil position at the output of the telescope. The position of the M3 active surface with respect to the rotating axis is also critical. The very tight tolerances on the distance between the M3 unit interface and the M3 axis are necessary to facilitate the integration of the M3 unit inside the mechanism without alignment.

The mechanism is extensively tested before the integration in the telescope. This is mostly done by using a CMM and a theodolite. The measured M3 axis radial run-out and the wobbling are $4\ \mu\text{m}$ and $4\ \text{arcsec}$ respectively.

The final alignment with respect to the inner axis is better than $5\ \text{arcsec}$ and $50\ \mu\text{m}$.

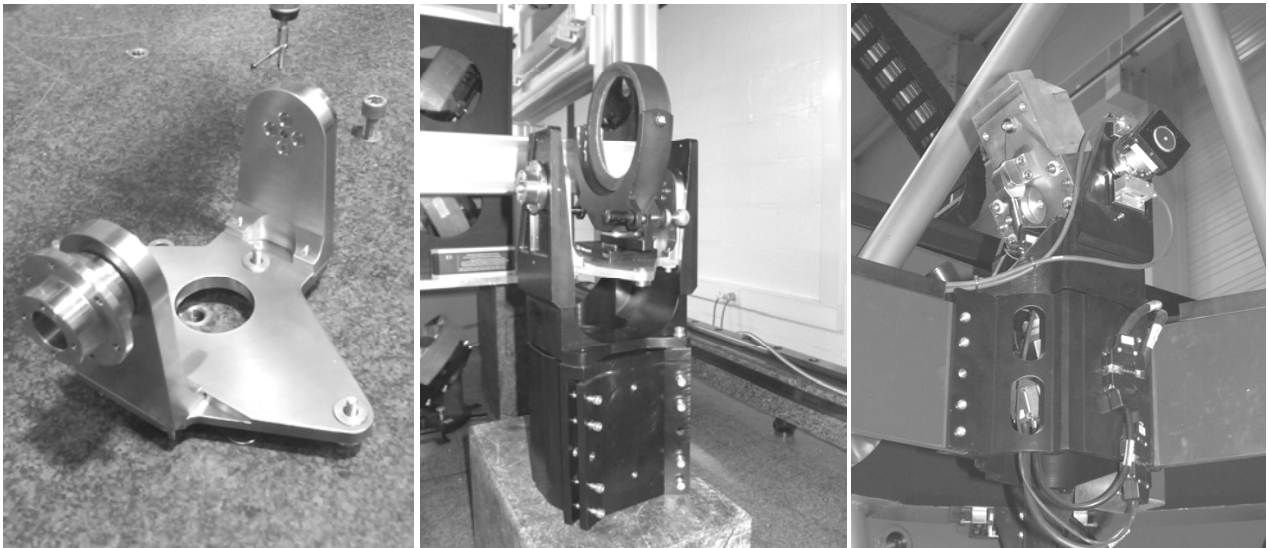


Figure 5. M3 mechanism: dimensional control, wobbling measurement and final alignment (from left to right)

3.3 Main axis balancing and friction measurement

Friction and unbalanced torque are estimated by measuring the motor torque during a backward and forward motion over the full stroke. The friction torque is half the difference between backward and forward torque values, while unbalanced torque is the mean of both torque values. Figure 6 shows outer axis torque measurement as a function of the axis position:

- Friction: between 100 and 140 Nm depending on axis position
- Unbalanced torque: 70 Nm. For safety reasons, the balancing of the axis has been tuned so that it is smaller than friction in any situation. The inner axis being embedded in the outer axis, it has to be balanced at first. Both axes are balanced along two planes parallel to the rotational axis. The resulting torque is:

$$T = a \cdot \sin(\theta) + b \cdot \cos(\theta) \quad [\text{Nm}] \quad (1)$$

- Disturbance torque due to motor cogging and ripple is a combination of 2 sine functions:

$$20 \cdot \sin(p \varphi) \quad [\text{Nm}] \quad (2)$$

$$23 \cdot \sin(2 p \varphi) \quad [\text{Nm}] \quad (3)$$

Where p is number of poles per turn

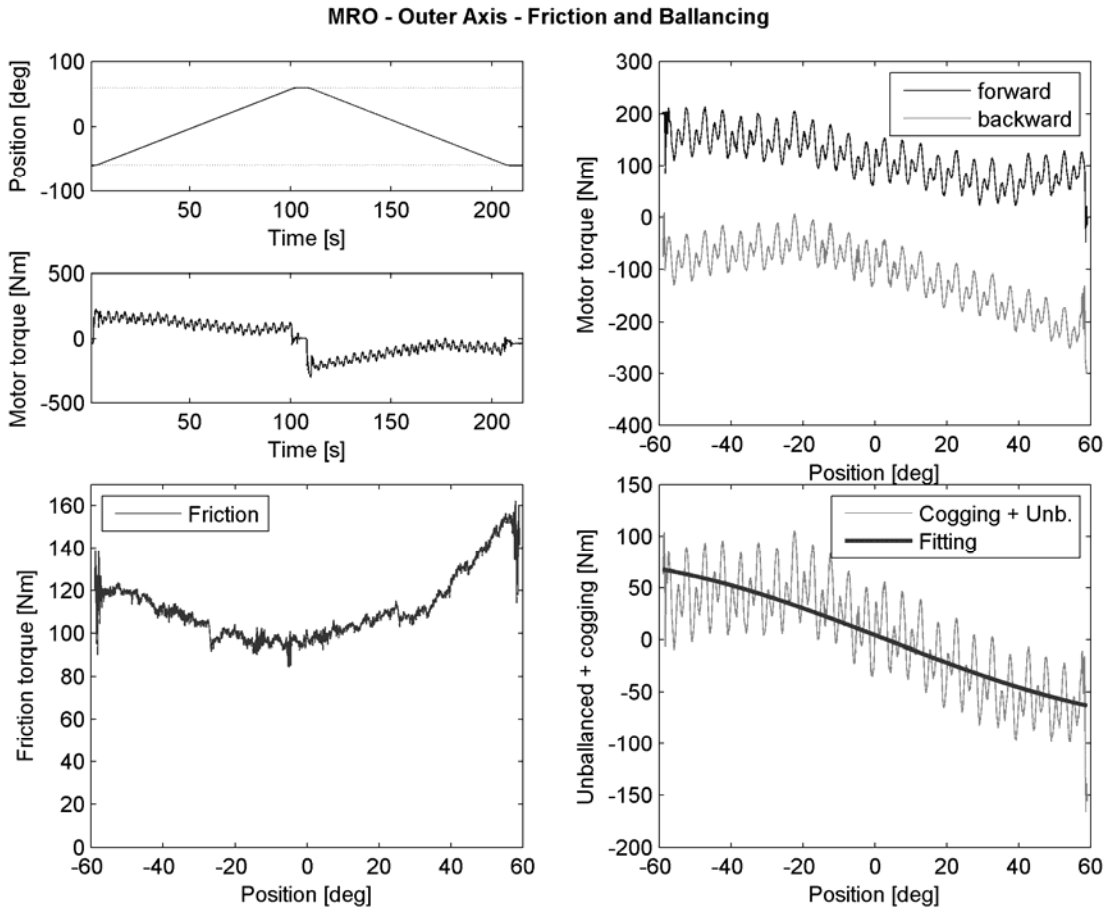


Figure 6. Measurement of friction and unbalanced torque of outer axis

3.4 System identification and main axis tuning

Open-loop transfer functions of inner and outer altitude axis have been measured using a white noise excitation. The measurement is performed with the axis controlled in closed-loop. A Compact DAQ (from National Instrument) is used to generate the white noise through a 16-bit UMAC input. It also acquires:

- 16-bit output of the UMAC controller (image of the current setpoint)
- Encoder position: one of the scanning head is connected to a IBV660B interpolator (from Heidenhain) that gives a 5V TTL signal which is read by the Compact DAQ to decode the axis position

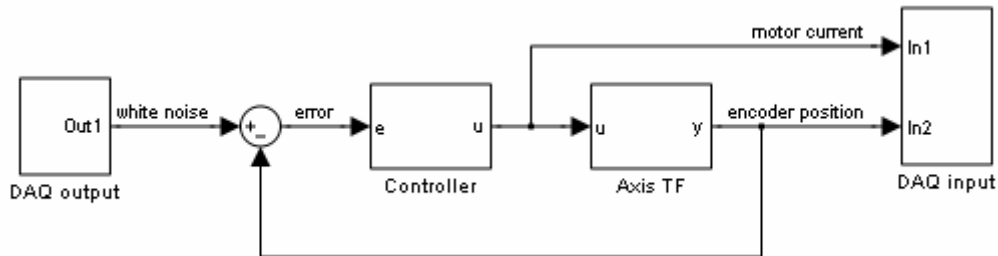


Figure 7. Identification set-up

The Open-loop transfer function (TFOL) is the frequency response function (FRF) between motor current and encoder position. This measurement is fit to an analytic transfer function with 22 poles and 22 zeros. Figure 2 shows the measurement and the identification performed with inner axis positioned at 40 deg from zenith and outer axis at 60 deg.

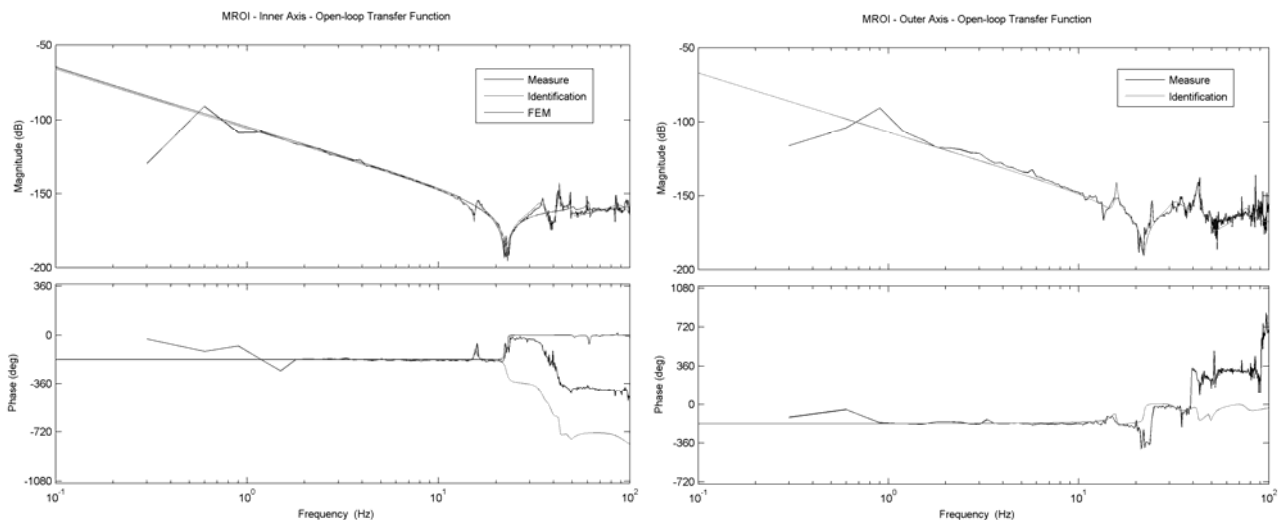


Figure 8. Open-loop transfer functions (Nm/rad)

It can be seen that the first resonance-anti resonance pair (13.5Hz - 15.8Hz) is a mode of the fork. The eigen-frequency with locked motors is 22.5Hz for inner axis and between 20.9 and 22.7Hz (depending of inner axis orientation) for outer axis. The 2 resonant frequencies observed at 35 and 43 Hz are present on both axes. The frequencies are lower than expected by the analysis because of the pier is not infinitely rigid.

UMAC standard algorithms consisting of proportional, integral, derivative terms and a second order filter are implemented in the controllers. The controllers have a position loop, a velocity loop and notch filters, so that several “UMAC controllers” have been used for each axis.

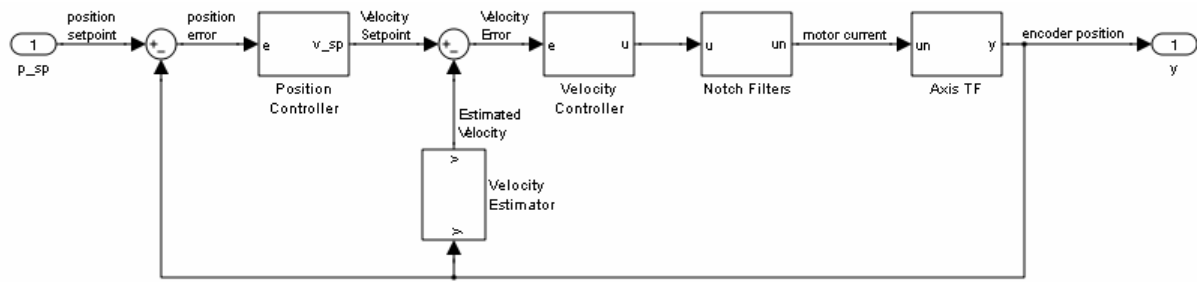


Figure 9. Controller architecture

Table 2. Controller configuration

	Inner Axis	Outer Axis
Position Loop	Proportional Integral Lead compensator (phase + 20 deg at 5Hz)	Proportional Integral Lead compensator (phase + 20 deg at 5Hz)
Velocity Loop	Proportional Integral Low-pass filter, cut-off frequency 40Hz, roll-off -40dB/dec	Proportional Integral Low-pass filter, cut-off frequency 30Hz, roll-off -40dB/dec
Velocity Estimator	Low-pass filter cut-off frequency 60Hz, roll-off -20dB/dec	Low-pass filter cut-off frequency 60Hz, roll-off -20dB/dec
Notch Filters	36Hz, 43Hz	15.5Hz, 36Hz, 43Hz

After fine tuning of the controllers, the closed-loop transfer functions and the servo performances are as presented in Figure 10 and Table 3 respectively. The evaluation of the tracking performances is performed in the frame of the factory acceptance test as discussed in section 4.3.

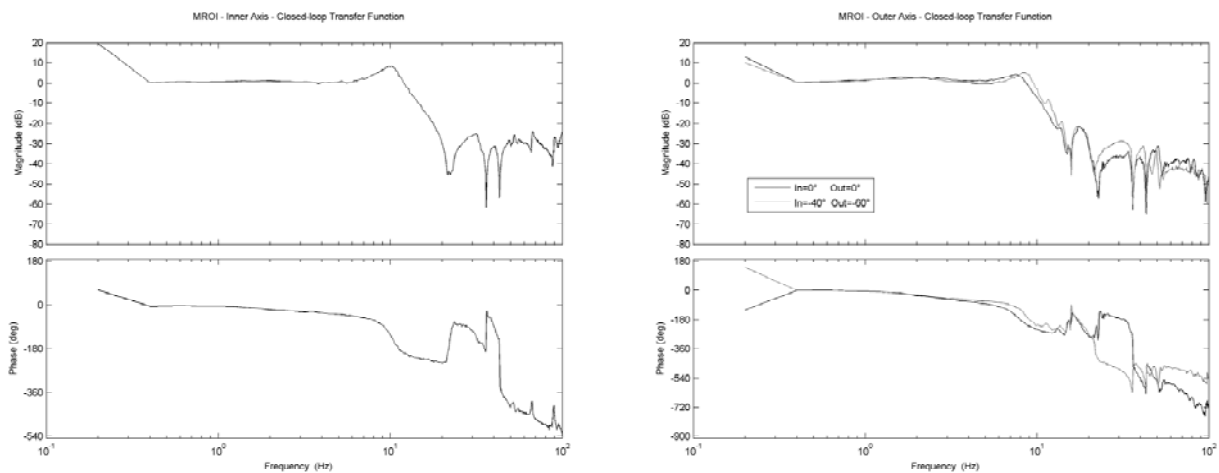


Figure 10: Closed-Loop transfer functions

Table 3. Servo performances

	Inner Axis		Outer Axis	
Position Loop	Bandwidth:	12.1Hz	Bandwidth:	9.2Hz
	Phase Margin:	45.2deg @ 7.3 Hz	Phase Margin:	48.2deg @ 4.04 Hz
	Gain Margin:	6.27dB @ 11.5Hz	Gain Margin:	6.54dB @ 8.66Hz
Velocity Loop	Bandwidth:	11.4Hz	Bandwidth:	10.4Hz
	Phase Margin:	60deg @ 7.13 Hz	Phase Margin:	52deg @ 6.27 Hz
	Gain Margin:	13.3dB	Gain Margin:	17.3dB

3.5 Wavefront sensor alignment

The Shack-Hartmann sensor is combined with a beam compressor. A folding mirror catches the output beam of the telescope and sends it to the beam compressor where it is resized to fit with the micro lens array. The water cooled camera and the lens array package is connected to the back of the beam compressor.

The Shack-Hartmann sensor was produced by OPTOCRAFT, Germany and thoroughly tested before shipment. The beam compressor was designed, assembled, aligned and tested at AMOS facilities. The system was tested against a flat reference. As the sensor provides relative measurement, the image quality requirement is not overly restrictive. The measured image quality including the folding mirror is 98 nm RMS compared to a budget of 400 nm RMS.

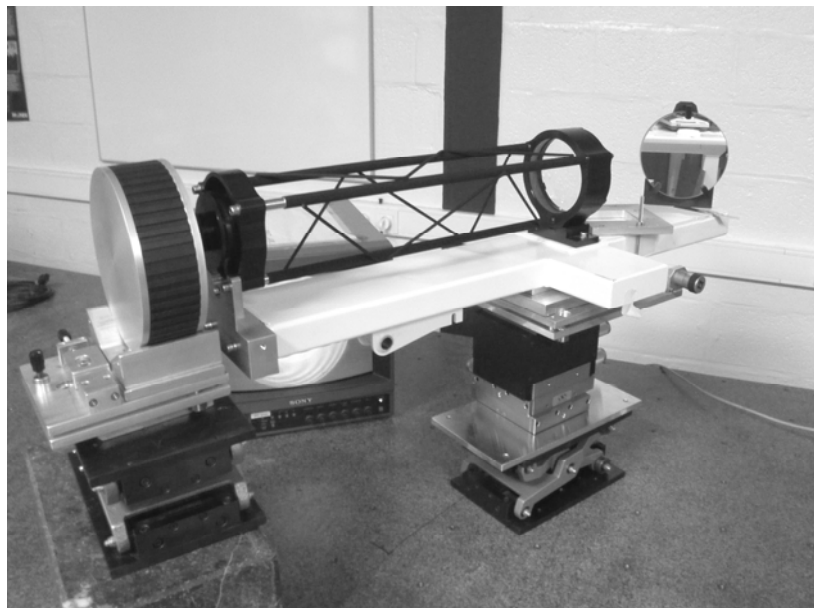


Figure 11. Beam compressor of the wavefront sensor under interferometric test

4. FACTORY ACCEPTANCE TEST

The requirements as specified by the customer are verified by design, inspection and test, or by a combination of the three methods. While the method of verification is imposed by the customer, the test procedures are defined by AMOS. The first step consists of establishing a plan a test is proposed in which for each requirement to verify with the following details: hardware configuration, test set-up, measurement accuracy and success criteria. Then, the detailed procedures including step by step operation, list of hardware and data processing techniques are written.

4.1 M2 mechanism performance

The M2 mechanism developed by Physik Instrumente, Germany is a key component of the system. The hexapod accuracy is critical for preserving the image quality. The fast tip-tilt actuator (FTTA) holding the secondary mirror is also critical because the system combines high dynamics for tracking performances with very low tilt-to-piston coupling at the level of the secondary mirror for OPL stability.

The mechanism has been exhaustively tested at sub-contractor premises. Only functional tests and FTFA bandwidth measurement were performed at AMOS after integration on the telescope.

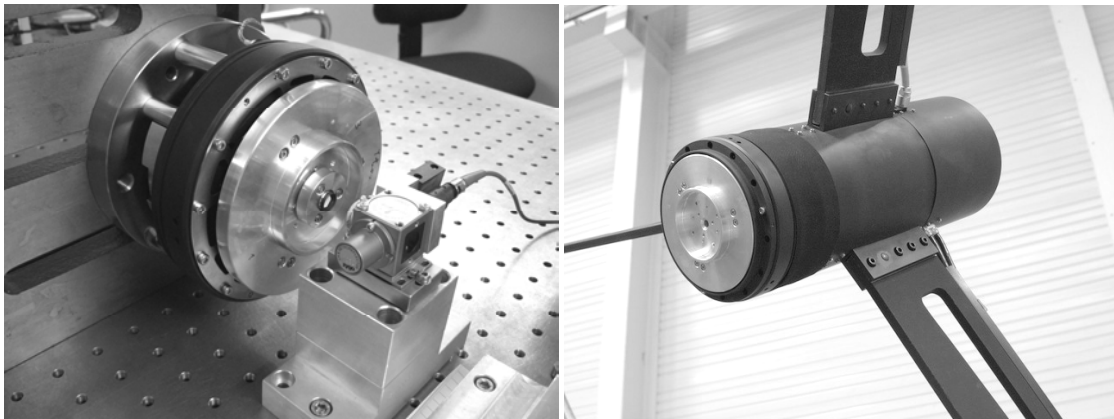


Figure 12. Tilt-to-piston coupling measurement set-up at PI premises (left) and M2 mechanism aligned in the telescope at AMOS (right)

The hexapod resolution and accuracy were measured by means of a laser interferometer and an electronic autocollimator with the mechanism placed vertically and horizontally. This means that the hexapod differential accuracy is evaluated for a given inclination of the system. The cross-talk generated by the motion of the other axis is taken into account in the calculation of the accuracy.

Table 4. Hexapod differential accuracy

	Specification	Measurement
tX	10 μm	6.9 μm
tY	10 μm	7.7 μm
tZ	2 μm	1.6 μm
rX	97 μrad	57 μrad
rY	97 μrad	50 μrad

The FTFA performances are measured with the mechanism placed vertically and horizontally on a rigid support. The tilt-to-piston coupling is measured by means of a single beam laser interferometer. The piston motion of the mirror is

produced by the inaccurate positioning of the optical surface vertex with respect to the FTTA pivot point and the vibrations generated by the piezo actuators.

The key point of the test set-up is the positioning of a corner cube exactly at the nominal M2 vertex of a dummy mirror having the same interface and mass characteristics as the real M2 mirror. The use of a laser tracker 0.5 inch corner cube is an effective method to locate the corner of the optical cube exactly at the desired position without adding significant mass to the dummy mirror.

The laser interferometer is used in a single beam configuration pointing toward the corner cube at the vertex of the dummy mirror. The system records linear displacements along the laser beam direction independently of the rotation around this point. The sampling rate of the measurement is 1 kHz and the resolution 0.62 nm.

The results presented in Table 5 shows that the piston motion is dominated by high frequency perturbations.

Table 5. M2 mechanism tilt-to-piston coupling

	Specification	Measurement
12 ms	23 nm RMS	20 nm RMS
17 ms	30 nm RMS	18 nm RMS
26 ms	44 nm RMS	17 nm RMS
35 ms	57 nm RMS	17 nm RMS
52 ms	78 nm RMS	16 nm RMS

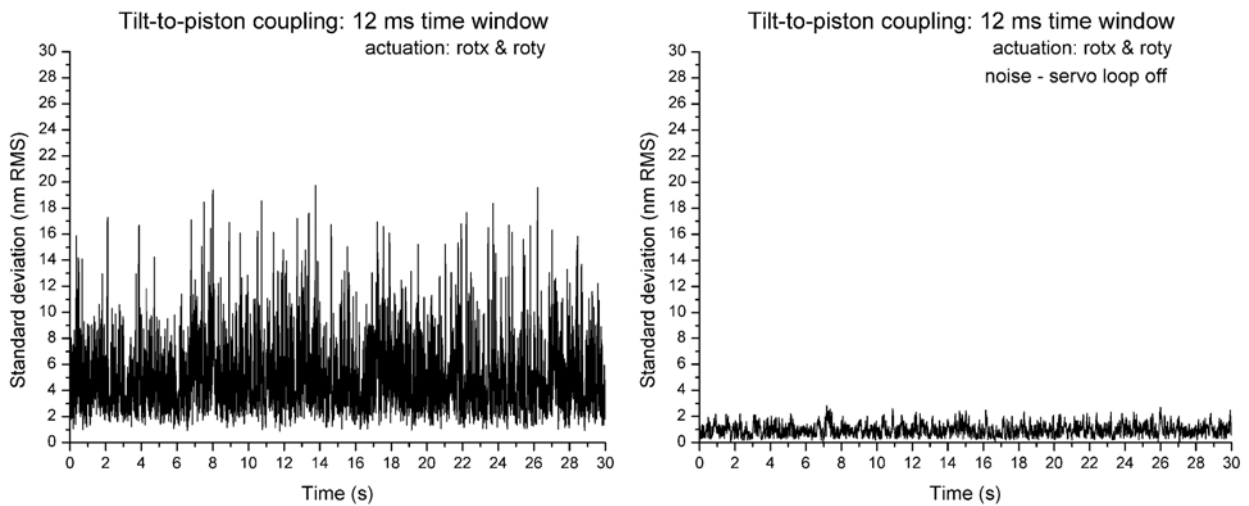


Figure 13. Tilt-to-piston coupling for 10 arcsec RMS of mirror physical rotation (tip and tilt)

The FTTA bandwidth is evaluated by dynamically measuring the rotation of the mirror by means of a vibrometer. The actual displacement is acquired and compared to the sine wave command to deduce the phase shift and the gain from 0.1 Hz to 200 Hz. The benefit of using active momentum compensation stage in the piezo platform appears clearly in Figure 14. The same test will be conducted at AMOS in order to ensure that the bandwidth of the system is not affected by the flexibility of the M2 spider.

Table 6. M2 FTTA phase shift at 50 Hz

	Specification	Measurement rX	Measurement rY
FTTA Xaxis down	-18 deg	-14.7 deg	-14.6 deg
FTTA Yaxis down	-18 deg	-13.7 deg	-13.5 deg
FTTA Zaxis down	-18 deg	-15.1 deg	-14.7 deg

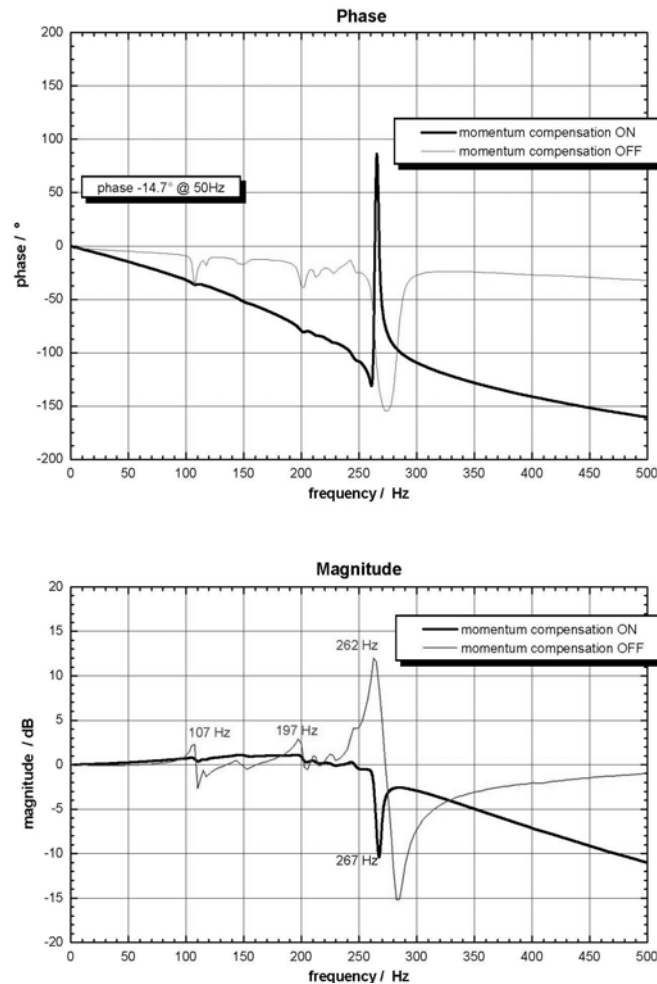


Figure 14. FTTA stiffness and phase shift

4.2 Telescope control system functionality

The UTCS has been designed with a number of features that facilitate verification. In particular it provides a well documented public interface that can be used to send commands and retrieve status, a comprehensive system for configuration that can be used whilst the control system is running plus facilities for introspection and logging.

System verification is structured around unit tests, system tests and acceptance tests. Unit tests are performed on individual components of the UTCS, system tests involve multiple components and acceptance tests are those that verify the requirements in the system specification. All tests are given a unique identifier and the acceptance tests are all traceable to the original requirements. As far as possible, tests are automated using scripts written in Python™. These

automated tests make full use of the public interface to the UTCS to both send commands and monitor for status changes. The use of Python™ allows arbitrarily complex tests to be written but we also auto generate some standard tests using the introspection built in to the system. For example all tests of the command interface are auto generated by extracting the full command list followed by the parameters and limits of each command. A script is then generated that tests the boundary values of all parameters of all commands.

Configuration data for each UTCS is stored in a configuration file that is loaded when the application is started. Some configuration data such as the ports and IP addresses on which the application listens for incoming connections are the same for each copy of the UTCS whereas other data e.g. the particular telescope’s pointing model will be different. All such configuration data is available when the control system is running through the ‘Parameter Manager’. The manager centralizes access to this data and provides the means for authorized users to inspect and change any item, restore the original default values, write a new configuration file and archive the previous one. The flexibility of this system along with the configurability of TCSpk has allowed the re-configuration of the alt-alt UTCS as a standard alt-az telescope and apply for example the full pointing model of Gemini North to verify that the demands to the drives for this re-configured system for a given astronomical target are the same as what the real Gemini control system produces.

Internal consistency of the control system has been checked by running dummy pointing tests. In these tests the UTCS is configured with a set of arbitrary pointing coefficients, a full pointing test is then run and the data logged and fitted with TPOINT. The results show that we can recover the input pointing model exactly in this test configuration. The re-configuration to an alt-az telescope and these dummy pointing tests give us confidence that there are no fundamental problems with the implementation of the control system.

Further verification of the correct operation of the system is available through the various system logs. Logs are automatically maintained of any state changes, particularly changes of health. A log is also maintained of all the data read from the PLC. Other logs can be configured as and when needed. For example it is possible to log all the data that passes over the public interface (by default only connections and disconnections are recorded). Each software component has a configurable debug level in the range 0 to 10 where increasing numbers provide increasing amounts of debug information. Finally, high speed logging of all the data from the UMAC on an axis by axis basis is possible.

4.3 Mount performance

The performances in wind-free environment are shown on Figure 15. The error (0.084 arcsec rms) is the combination of inner axis, outer axis and M3 mechanism. When filtered by the FTTA, the error is reduced to 0.008 arcsec rms.

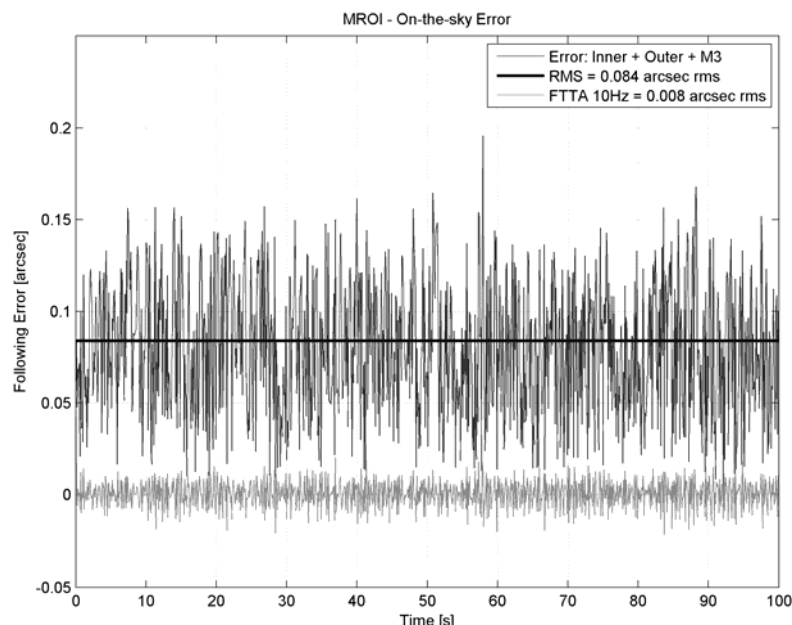


Figure 15. Mount error in wind free environment

While the performances in wind-free environment are determined both by analysis and by measurement, the contribution of the wind disturbance can be evaluated only by analysis.

The Von Karman wind model is used for this analysis. It gives the one-sided power spectral density (PSD) of wind speed:

$$S_U(f) = (IU)^2 \cdot \frac{4L}{U} \cdot \frac{1}{(1 + 70.78 \frac{L^2}{U^2} f^2)^{5/6}} \quad (4)^2$$

where:

- S_U is the power spectral density of the wind speed [(m/s)²/Hz]
- I is the turbulence intensity
- U is the mean speed of the wind outside the dome [m/s]
- L is the length scale of turbulence [m]
- f is the considered frequency [Hz]

In the present analysis, the mean speed is 10 m/s, the turbulence intensity is 0.12 and the length scale equals 5 m

Figure 16 shows for inner axis:

- Wind PSD of Von Karman model
- Transfer function of torque disturbance rejection
- Wind shake residual (tracking error of the axis due to wind disturbance) when the telescope operates with optical feedback. It is calculated as follow:

$$y_{rms} = \sqrt{\int_0^{\infty} PSD(f) \cdot [NR(f) \cdot \frac{s}{s + 2\pi f_{-3dB}}]^2 df} \quad (5)$$

where f_{-3dB} is 0.1 Hz for the guider and up to 50 Hz for the fast tip-tilt system.

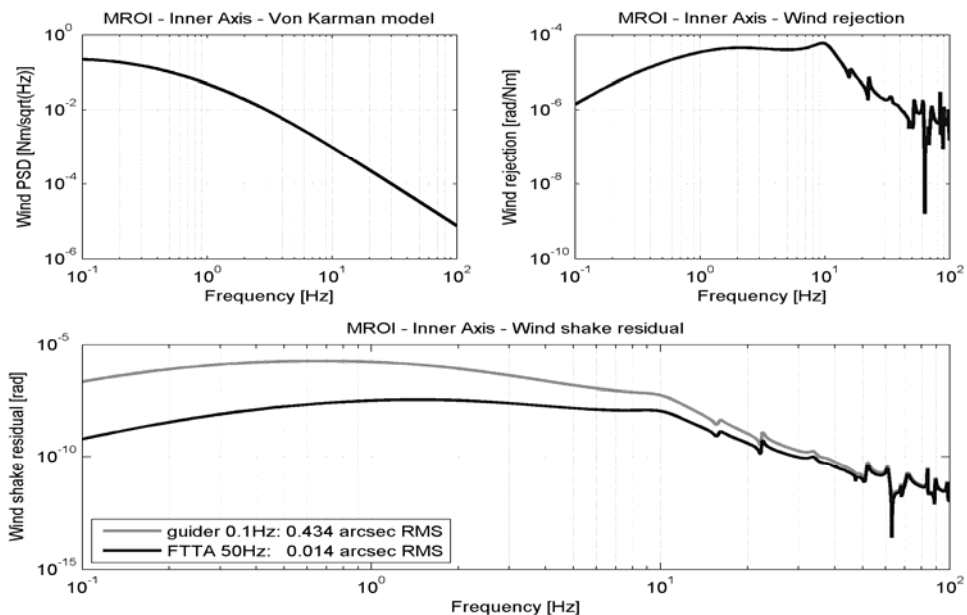


Figure 16. Wind shake residuals

4.4 Optical path length stability

The instrumental perturbation of OPL stability has to be kept as low as possible. The requirement for the unit telescope concerns the variation of the OPL from the star to the output of M3 during short time windows corresponding to the exposure time of the interferometric instrument. The identified contributors to the OPL variation are the vibrations resulting from the dynamic wind load, the normal micro-seismic activity, the enclosure and telescope active sources during operation. The OPL variation was a key parameter of the telescope mechanical design where optimization processes were necessary to fulfil the requirement specification. The OPL test aims to assess the *weight* of the telescope internal vibration on the total OPL stability budget given in Table 7.

The OPL variation from the telescope output backward to the primary mirror is measured by means of a single beam laser interferometer. The optical beam is reflected on flat dummies M3 and M2 representative of the mass of the real mirrors. A corner cube installed on the dummy primary mirror near the center sends the beam back to the interferometric cube situated next to the Nasmyth table. The set-up will measure 4 times the displacement of M2 and M3 but only 2 times the displacement of M1. Consequently, it is necessary to measure the displacement of the primary simultaneously by another way. This is done by means of a seismic interferometer rigidly connected to the dummy M1 nearby the retro-reflector.

The measurement equipment provided correlated acceleration time histories. The OPL variation from the star to the telescope output is related to the acceleration $a = \frac{1}{2} a_{HP} - a_{M1}$ where a_{HP} and a_{M1} are respectively the acceleration measured by means of the interferometer and the accelerometer. The power spectral density (PSD) of the displacement is given by integrating twice the acceleration PSD. The RMS position error σ during the exposure time τ is computed using the formula:

$$\sigma^2(\tau) = \int_{1\text{Hz}}^{\text{Nyquist}} \text{PSD}(f) [1 - \text{sinc}^2(\tau f)] df \quad (6)$$

The acquisition duration is 30 sec at a sampling rate of 1 kHz. Measurements are made for various tracking speeds. The background is measured when all the devices are powered off, and this level is removed from the measurement by a quadratic difference.

Beyond the OPL stability expressed in nm RMS, the frequency domain processing contributed to a better understanding of the system. Indeed, the dominant internal sources of vibration of the telescope can be identified by comparison of the displacement PSD for different measurement configurations.

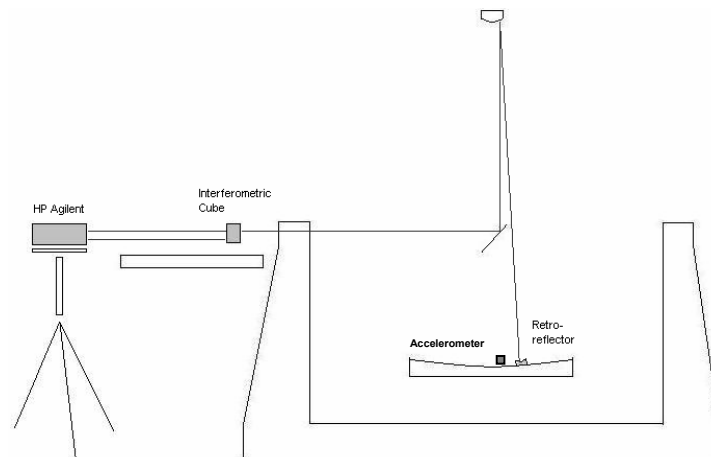


Figure 17. Wind shake residuals

Table 7. Maximum allowed vibration-induced pathlength fluctuations

Time interval	Specification
12 ms	23 nm RMS
17 ms	30 nm RMS
26 ms	44 nm RMS
35 ms	57 nm RMS
52 ms	78 nm RMS

4.5 Pupil stability

The output pupil position is defined as the position of the centre of the image of the telescope primary mirror as seen through the combination of the secondary and tertiary mirrors (the projected telescope pupil image) from a location mechanically independent of the telescope.

The stability of each exit pupil during observation is critical as the fringes visibility depends on the overlapping surface of the combined UT pupils. Matching between UT exit pupils and beam combiner entrance pupil is also a critical aspect in order to prevent vignetting. It is required that the pupil position of each unit telescope varies by less than $\pm 0.5\text{mm}$ over the operational field of regard.

As the pupil imaged by the M2 is located close to the M2, the factory acceptance test consists of measuring the relative displacement of a target bonded on the M2 dummy seen through the M3. The set-up consists of a 16 Megapixel Prosilica CCD coupled to a 800 mm fixed focal objective. The objective is installed on a stable support at the output of the telescope and is sighting the target at the level of M2. A dedicated software application captures the image, calculates the centroid and stores the data in log file. The pupil position is calculated for at least 24 pointing directions evenly distributed in the FOR. The data set allows the determination of the required adjustment of the M2 and M3 for minimizing the pupil motion. Afterwards, the parameters for the M2 compensation law can be determined. At the end, the test is carried out again while the M2 position compensates for the pupil position. This last test exhibits the greatest pupil stability.

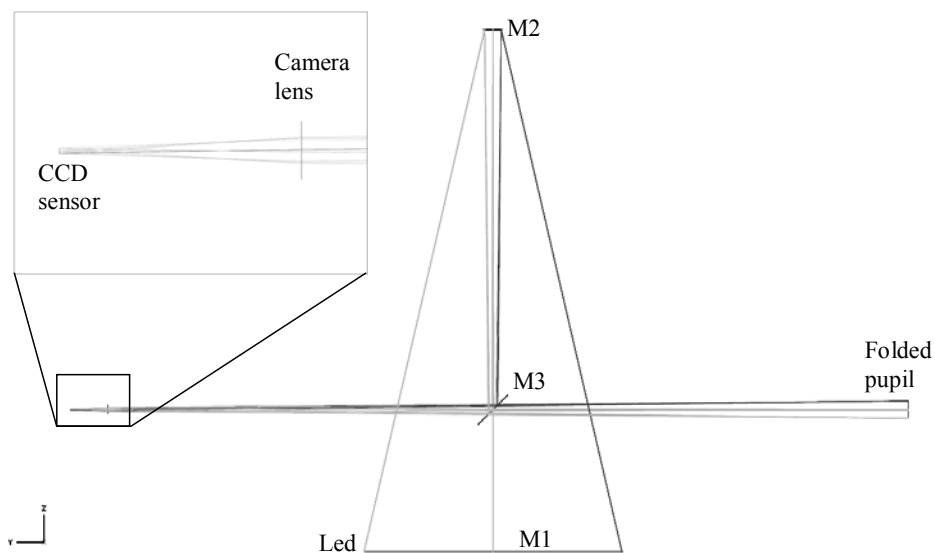


Figure 18. Pupil stability test set-up

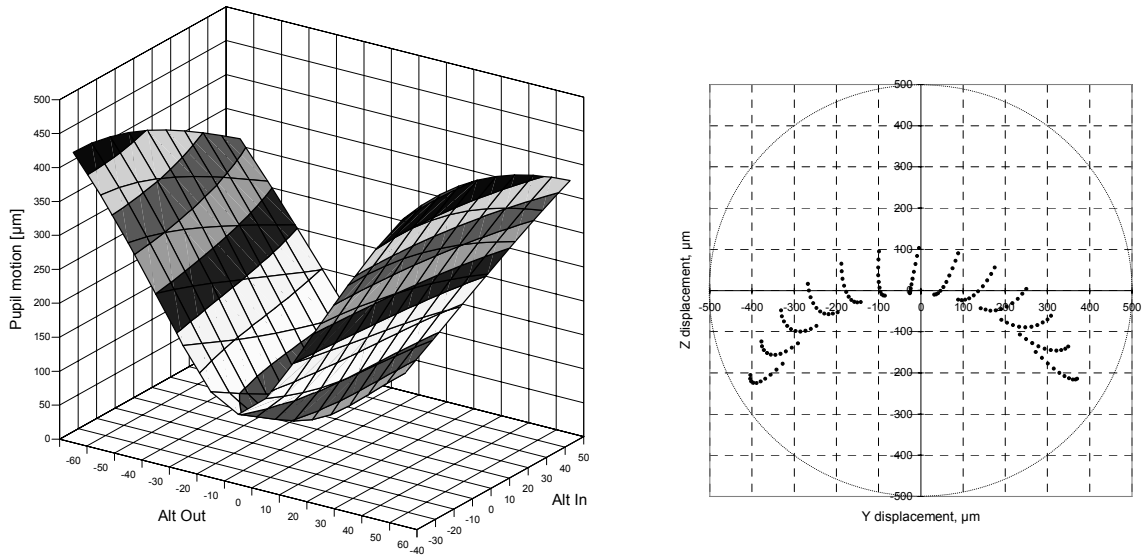


Figure 19. Pupil motion expected (M3 run-out = $4\mu\text{m}$ and main axes run-out = $15\mu\text{m}$)

5. CONCLUSIONS

An overview of the alignment and testing activities performed on the *as built* unit telescope have been presented. The performances and functionalities are verified by test not only because it is required by the customer but also on account that this is the only way to drastically reduce the risk of major difficulty during on-site installation and commissioning.

For more than 25 years, AMOS has acquired a valuable experience in assembly, integration and testing. As during the design phases of the projects, the strength of AMOS originates from the combination of skills and knowledge in optical, mechanical, thermal, mechatronic and software fields.

REFERENCES

- [1] Buscher, D. F., Bakker, E. J., Coleman, T. A., et al., "The Magdalena Ridge Observatory Interferometer: a high sensitivity imaging array," Proc. SPIE 6307, - (2006)
- [2] Pirnay, O., Gloesener, P., Gabriel, E., Graillet, F. and Delrez, Ch., "Design of the unit telescopes of the MROI," Proc. SPIE 7013, - (2008)
- [3] Mayer, C. J., et al., "The control system for the unit telescopes of the Magdalena Ridge Observatory interferometer," Proc. SPIE 7019, - (2008)